

A novel technique for modelling interfaces in reinforced brittle materials

A. Simone, G. N. Wells & L. J. Sluys

Koiter Institute Delft, Delft University of Technology, The Netherlands

ABSTRACT: A novel numerical technique for the modelling of interfaces is introduced for the analysis of reinforced brittle materials. The method exploits the partition of unity property of finite element shape functions. By considering finite element shape functions as partitions of unity, extra degrees of freedom are added to the nodes at the interface between the matrix and reinforcement. A gradient-enhanced damage model is used to simulate the continuum response. Numerical results for a three-point bending test and a pull-out test are presented. The numerical procedure proposed here is suitable for a great variety of applications ranging from discrete cracking and steel-concrete interaction in concrete to delamination processes in composite materials.

1 INTRODUCTION

For the computational modelling of interface phenomena, special elements are required to simulate relative movement between two surfaces. Interface elements allow such phenomena to be captured and they are widely used for the modelling of discontinuities in materials. Fields of application are, for instance, concrete mechanics, for the description of the interface between steel and concrete, and modelling of delamination processes in layered composites.

A critical point in the proper use of standard interface elements is the choice of the mechanical properties. Ideally, no deformation should occur at an interface in the elastic stage of loading. Standard interface elements fail in this respect as they need an initial elastic stiffness (Rots 1988). Moreover, the presence of spurious oscillations in the stress field makes non-linear computations which are performed with standard interface elements very sensitive.

Recently, different numerical techniques have been developed which allow displacement discontinuities to pass through solid finite elements. It is then possible to describe crack propagation without remeshing, with the path of the discontinuity independent of the spatial discretisation. The technique proposed here makes use of the partition of unity property of finite element shape functions (the sum of the shape functions must equal unity at each spatial point) noted by Melenk and Babuška (1996). The essential idea in this method is to extend the standard approximation basis with enriched functions. This enhancement results in extra degrees of freedom for an enriched node, without modification of the mesh topology. In this pa-

per, following Wells and Sluys (2001b), the standard FEM polynomial basis is enriched with discontinuous functions. This approach has been successfully applied for the analysis of quasi-static (Wells and Sluys 2001b) and dynamic (Wells and Sluys 2001a) failure in quasi-brittle materials. Unlike the model proposed by Wells and Sluys (2001b), in which a propagating discontinuity is allowed to cross through solid finite elements, the model proposed here considers a discontinuity whose location is known *a priori*.

For interface modelling, a discontinuity may develop at the common boundary of concrete matrix and reinforcement. The model results in an interface-like element in which extra degrees of freedom are activated on nodes lying on a discontinuity. A bond-slip constitutive law is used at the discontinuity.

Inelastic deformations in the concrete matrix are represented using a continuum damage model. To avoid dependence on the spatial discretisation an enhanced continuum description is necessary. Here, the inclusion of higher-order spatial derivatives (Peerlings 1999) is used. Numerical simulations of a three-point bending test and a pull-out test highlight the properties of the method and its ability to overcome the difficulties encountered when using standard interface elements.

2 KINEMATIC FIELDS

A body Ω bounded by Γ and crossed by a discontinuity Γ_d is considered (see Figure 1). Prescribed displacements are imposed on Γ_u , while tractions are imposed on Γ_t . The internal discontinuity surface Γ_d divides the body into two sub-domains, Ω^+ and Ω^-

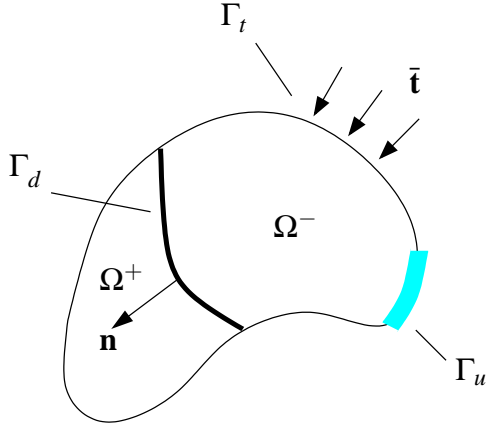


Figure 1: Body Ω crossed by a discontinuity Γ_d .

($\Omega = \Omega^+ \cup \Omega^-$). The displacement field can be described by

$$\mathbf{u}(\mathbf{x}, t) = \hat{\mathbf{u}}(\mathbf{x}, t) + \mathcal{H}_{\Gamma_d}(\mathbf{x}) \tilde{\mathbf{u}}(\mathbf{x}, t), \quad (1)$$

where $\mathcal{H}_{\Gamma_d}(\mathbf{x})$ is the Heaviside function centred at the discontinuity surface Γ_d ($\mathcal{H}_{\Gamma_d} = 1 \forall \mathbf{x} \in \Omega^+$, $\mathcal{H}_{\Gamma_d} = 0 \forall \mathbf{x} \in \Omega^-$) and $\hat{\mathbf{u}}$ and $\tilde{\mathbf{u}}$ are continuous functions on Ω . Note that the displacement jump is given by $\tilde{\mathbf{u}}$ at the discontinuity surface Γ_d . The corresponding strain field is obtained as the symmetric part of the gradient of the displacement field:

$$\boldsymbol{\varepsilon} = \nabla^s \mathbf{u} = \nabla^s \hat{\mathbf{u}} + \mathcal{H}_{\Gamma_d} (\nabla^s \tilde{\mathbf{u}}) + \delta_{\Gamma_d} (\tilde{\mathbf{u}} \otimes \mathbf{n})^s, \quad (2)$$

where $(\cdot)^s$ refers to the symmetric part of (\cdot) , δ_{Γ_d} is the Dirac delta-function centred at the discontinuity Γ_d and \mathbf{n} is the unit normal vector to the discontinuity (pointing to Ω^+). Due to the jump in the displacement field, the strain at the discontinuity is unbounded. This lacks physical meaning and it will be eliminated analytically from the virtual work equation.

3 FINITE ELEMENT IMPLEMENTATION

3.1 Kinematic description

In a finite element framework, the kinematic field must be described in terms of nodal values. The displacement field in equation (1) is expressed as

$$\mathbf{u} = \mathbf{N}\mathbf{a} + \mathcal{H}_{\Gamma_d} \mathbf{N}\mathbf{b}, \quad (3)$$

where \mathbf{N} is a matrix containing element shape functions and \mathbf{a} and \mathbf{b} represent regular and enhanced nodal degrees of freedom, respectively. The discretisation for the strain field reads:

$$\boldsymbol{\varepsilon} = \mathbf{B}\mathbf{a} + \mathcal{H}_{\Gamma_d} \mathbf{B}\mathbf{b} + \left(\delta_{\Gamma_d} \mathbf{n} \right) \mathbf{N}\mathbf{b}, \quad (4)$$

where the gradients in equation (2) have been expressed as $\nabla^s \hat{\mathbf{u}} = \mathbf{B}\mathbf{a}$ and $\nabla^s \tilde{\mathbf{u}} = \mathbf{B}\mathbf{b}$, with the matrix \mathbf{B} containing the spatial derivatives of the element shape functions and \mathbf{n} is a matrix containing normal components to the discontinuity.

3.2 Variational formulation

The variational formulation follows Wells and Sluys (2001b). The virtual work equation, without body forces, reads:

$$\int_{\Omega} \nabla^s \boldsymbol{\eta} : \boldsymbol{\sigma} \, d\Omega = \int_{\Gamma_t} \boldsymbol{\eta} \cdot \bar{\mathbf{t}} \, d\Gamma, \quad (5)$$

where $\boldsymbol{\eta}$ are admissible displacement variations, $\boldsymbol{\sigma}$ is the stress field and $\bar{\mathbf{t}}$ are external traction forces on the boundary Γ_t . From equation (1), the displacement variation $\boldsymbol{\eta}$ is decomposed as

$$\boldsymbol{\eta} = \hat{\boldsymbol{\eta}} + \mathcal{H}_{\Gamma_d} \tilde{\boldsymbol{\eta}}. \quad (6)$$

From equation (2), the symmetric part of the gradient of $\boldsymbol{\eta}$ is equal to

$$\nabla^s \boldsymbol{\eta} = \nabla^s \hat{\boldsymbol{\eta}} + \mathcal{H}_{\Gamma_d} \nabla^s \tilde{\boldsymbol{\eta}} + \delta_{\Gamma_d} (\tilde{\boldsymbol{\eta}} \otimes \mathbf{n})^s. \quad (7)$$

Substituting the admissible displacement variation (6) and its gradient (7) into the virtual work equation (5) gives:

$$\begin{aligned} & \int_{\Omega} \nabla^s \hat{\boldsymbol{\eta}} : \boldsymbol{\sigma} \, d\Omega + \int_{\Omega} \mathcal{H}_{\Gamma_d} \nabla^s \tilde{\boldsymbol{\eta}} : \boldsymbol{\sigma} \, d\Omega \\ & + \int_{\Omega} \delta_{\Gamma_d} (\tilde{\boldsymbol{\eta}} \otimes \mathbf{n})^s : \boldsymbol{\sigma} \, d\Omega = \int_{\Gamma_t} \left(\hat{\boldsymbol{\eta}} + \mathcal{H}_{\Gamma_d} \tilde{\boldsymbol{\eta}} \right) \cdot \bar{\mathbf{t}} \, d\Gamma. \end{aligned} \quad (8)$$

Using the integral property of the Dirac-delta distribution,

$$\begin{aligned} & \int_{\Omega} \delta_{\Gamma_d} (\tilde{\boldsymbol{\eta}} \otimes \mathbf{n})^s : \boldsymbol{\sigma} \, d\Omega \\ & = \int_{\Gamma_d} (\tilde{\boldsymbol{\eta}} \otimes \mathbf{n})^s : \boldsymbol{\sigma} \, d\Gamma = \int_{\Gamma_d} \tilde{\boldsymbol{\eta}} \cdot \mathbf{t} \, d\Gamma, \end{aligned} \quad (9)$$

where $\mathbf{t} = \boldsymbol{\sigma}\mathbf{n}$ are the traction forces acting across the discontinuity Γ_d . Inserting equation (9) into equation (8), the weak form reads:

$$\begin{aligned} & \int_{\Omega} \nabla^s \hat{\boldsymbol{\eta}} : \boldsymbol{\sigma} \, d\Omega + \int_{\Omega} \mathcal{H}_{\Gamma_d} \nabla^s \tilde{\boldsymbol{\eta}} : \boldsymbol{\sigma} \, d\Omega \\ & + \int_{\Gamma_d} \tilde{\boldsymbol{\eta}} \cdot \mathbf{t} \, d\Gamma = \int_{\Gamma_t} \left(\hat{\boldsymbol{\eta}} + \mathcal{H}_{\Gamma_d} \tilde{\boldsymbol{\eta}} \right) \cdot \bar{\mathbf{t}} \, d\Gamma. \end{aligned} \quad (10)$$

From the decomposition of the displacement field it follows that any admissible variation $\boldsymbol{\eta}$ of \mathbf{u} can be regarded as admissible variations $\hat{\boldsymbol{\eta}}$ and $\tilde{\boldsymbol{\eta}}$, thus leading

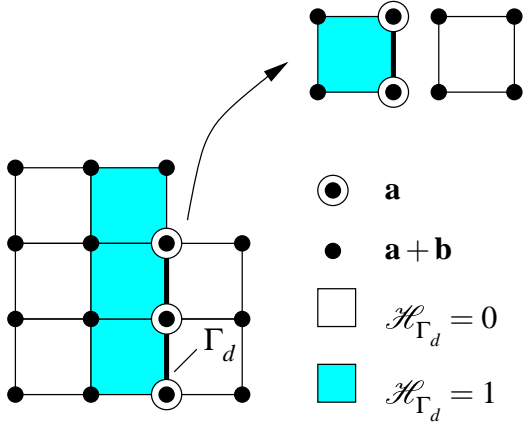


Figure 2: Enhanced nodes lying on a discontinuity.

to two variational statements. Taking first variation $\hat{\boldsymbol{\eta}}$ and then $\tilde{\boldsymbol{\eta}}$ gives:

$$\int_{\Omega} \nabla^s \hat{\boldsymbol{\eta}} : \boldsymbol{\sigma} \, d\Omega = \int_{\Gamma_t} \hat{\boldsymbol{\eta}} \cdot \bar{\mathbf{t}} \, d\Gamma \quad (11a)$$

$$\int_{\Omega} \mathcal{H}_{\Gamma_d} \nabla^s \tilde{\boldsymbol{\eta}} : \boldsymbol{\sigma} \, d\Omega + \int_{\Gamma_d} \tilde{\boldsymbol{\eta}} \cdot \mathbf{t} \, d\Gamma = \int_{\Gamma_t} \mathcal{H}_{\Gamma_d} \tilde{\boldsymbol{\eta}} \cdot \bar{\mathbf{t}} \, d\Gamma. \quad (11b)$$

Note that the second variational statement ensures that traction continuity is satisfied in a weak sense across the discontinuity Γ_d .

3.3 Spatial discretisation

Due to the presence of two materials, a discontinuity is added at the boundary between concrete matrix and reinforcement. While an interface lies at the boundary between two elements, the discontinuity *belongs* to the element upon which $\mathcal{H}_{\Gamma_d} = 1$. This is illustrated in Figure 2, in which the shaded elements, sharing a common boundary with the white elements, contain a discontinuity placed along the common side. It is emphasized that the enhancement regards only those nodes of interface-like elements (the shaded elements in Figure 2) lying on a discontinuity.

For elements with a discontinuity, it is convenient to define the discretised expressions for the admissible displacement jump variations and their gradients as $\mathcal{H}_{\Gamma_d} \hat{\boldsymbol{\eta}} = \mathbf{N}_{\mathcal{H}} \mathbf{b}'$ and $\mathcal{H}_{\Gamma_d} \nabla^s \hat{\boldsymbol{\eta}} = \mathbf{B}_{\mathcal{H}} \mathbf{b}'$, respectively, where the primes refer to variations. The matrices $\mathbf{N}_{\mathcal{H}}$ and $\mathbf{B}_{\mathcal{H}}$ are such that only the contribution of the nodes lying on the discontinuity are considered. Defining analogous expressions for the admissible displacement variations ($\hat{\boldsymbol{\eta}} = \mathbf{N} \mathbf{a}'$ and $\tilde{\boldsymbol{\eta}} = \mathbf{N} \mathbf{b}'$) and for their gradients ($\nabla^s \hat{\boldsymbol{\eta}} = \mathbf{B} \mathbf{a}'$ and $\nabla^s \tilde{\boldsymbol{\eta}} = \mathbf{B} \mathbf{b}'$), and inserting these expressions into equation (11), leads to two discrete weak governing equations valid at element level:

$$\int_{\Omega^+} \mathbf{B}^T \boldsymbol{\sigma} \, d\Omega = \int_{\Gamma_t} \mathbf{N}^T \bar{\mathbf{t}} \, d\Gamma \quad (12a)$$

$$\int_{\Omega^+} \mathbf{B}_{\mathcal{H}}^T \boldsymbol{\sigma} \, d\Omega + \int_{\Gamma_d} \mathbf{N}^T \mathbf{t} \, d\Gamma = \int_{\Gamma_t} \mathbf{N}_{\mathcal{H}}^T \bar{\mathbf{t}} \, d\Gamma. \quad (12b)$$

The requirement of zero enhanced displacement ($\tilde{\mathbf{u}} = \mathbf{0}$) is enforced where essential boundary conditions are applied (Wells and Sluys 2001b). From equation (12), the equivalent nodal forces related to admissible variations of \mathbf{a} and \mathbf{b} result in

$$\mathbf{f}_{\text{int},a} = \int_{\Omega^+} \mathbf{B}^T \boldsymbol{\sigma} \, d\Gamma \quad (13a)$$

$$\mathbf{f}_{\text{int},b} = \int_{\Omega^+} \mathbf{B}_{\mathcal{H}}^T \boldsymbol{\sigma} \, d\Omega + \int_{\Gamma_d} \mathbf{N}^T \mathbf{t} \, d\Gamma. \quad (13b)$$

3.4 Linearised weak equations

The stress rate $\dot{\boldsymbol{\sigma}}$ in the continuum is expressed in terms of nodal displacement velocities as

$$\dot{\boldsymbol{\sigma}} = \mathbf{D} \dot{\boldsymbol{\varepsilon}} = \mathbf{D} (\mathbf{B} \dot{\mathbf{a}} + \mathbf{B}_{\mathcal{H}} \dot{\mathbf{b}}), \quad (14)$$

where the material tangent \mathbf{D} links stress rate $\dot{\boldsymbol{\sigma}}$ to strain rate $\dot{\boldsymbol{\varepsilon}}$. Similarly, the traction rate at a discontinuity is expressed as

$$\dot{\mathbf{t}} = \mathbf{T}[\dot{\mathbf{u}}] = \mathbf{T} \mathbf{N} \dot{\mathbf{b}}, \quad (15)$$

where \mathbf{T} relates traction rate $\dot{\mathbf{t}}$ and displacement jump rate $[\dot{\mathbf{u}}]$. The linearised weak form is formed by inserting the above stress and traction rate expressions into the discretised weak governing equations in equation (12), thus obtaining

$$\begin{bmatrix} \mathbf{K}_{aa} & \mathbf{K}_{ab} \\ \mathbf{K}_{ba} & \mathbf{K}_{bb} \end{bmatrix} \begin{bmatrix} \Delta \mathbf{a} \\ \Delta \mathbf{b} \end{bmatrix} = \begin{bmatrix} \mathbf{f}_{\text{ext},a}^{t+dt} \\ \mathbf{f}_{\text{ext},b}^{t+dt} \end{bmatrix} - \begin{bmatrix} \mathbf{f}_{\text{int},a}^t \\ \mathbf{f}_{\text{int},b}^t \end{bmatrix}, \quad (16)$$

where the sub-matrices are defined as

$$\mathbf{K}_{aa} = \int_{\Omega^+} \mathbf{B}^T \mathbf{D} \mathbf{B} \, d\Omega \quad (17a)$$

$$\mathbf{K}_{ab} = \int_{\Omega^+} \mathbf{B}^T \mathbf{D} \mathbf{B}_{\mathcal{H}} \, d\Omega \quad (17b)$$

$$\mathbf{K}_{ba} = \int_{\Omega^+} \mathbf{B}_{\mathcal{H}}^T \mathbf{D} \mathbf{B} \, d\Omega \quad (17c)$$

$$\mathbf{K}_{bb} = \int_{\Omega^+} \mathbf{B}_{\mathcal{H}}^T \mathbf{D} \mathbf{B}_{\mathcal{H}} \, d\Omega + \int_{\Gamma_d} \mathbf{N}^T \mathbf{T} \mathbf{N} \, d\Omega \quad (17d)$$

and \mathbf{f}_{ext} are the externally applied forces (RHS of equation (12)).

4 INTERFACE CONSTITUTIVE MODELS

The traction-separation relation $\dot{\mathbf{t}} = \mathbf{T}[\dot{\mathbf{u}}]$ of equation (15) is formulated in a local n,s coordinate system. To test the model and to make comparisons with standard interface element problems, a simple law of the type

$$\begin{bmatrix} \dot{t}_n \\ \dot{t}_s \end{bmatrix} = \begin{bmatrix} d_n & 0 \\ 0 & d_s \end{bmatrix} \begin{bmatrix} \dot{\tilde{u}}_n \\ \dot{\tilde{u}}_s \end{bmatrix} \quad (18)$$

is used, where d_n and d_s are constant, \tilde{u}_n and \tilde{u}_s are the displacement jumps in the local (discontinuity) reference system and t_n and t_s are the normal and tangential interface tractions.

A more refined model is required for the description of pull-out failure. A loading function is defined as

$$f(\tilde{u}_s, \kappa) = \tilde{u}_s - \kappa, \quad (19)$$

where κ is a history parameter, equal to the largest value of \tilde{u}_s reached. Loading is indicated by $f \geq 0$ and unloading by $f < 0$.

The constitutive response along the common boundary of reinforcement and matrix has been idealised considering a damaging interface in which

$$t_s = d_s(1 - \omega_s)\kappa, \quad (20)$$

where ω_s is the tangential damage factor. A perfect normal bond is assumed. For the tangential traction-slip relationship, a linear softening damage evolution law is used:

$$\omega_s = 1 - \frac{\kappa_i}{\kappa} \left(\frac{\kappa_u - \kappa}{\kappa_u - \kappa_i} \right), \quad (21)$$

which is characterised, after the threshold value κ_i has been reached, by a linear decrease of the tangential traction until a zero tangential traction level is reached for the ultimate slip κ_u . Secant unloading is adopted.

5 IMPLEMENTATION

The model has been implemented using four- and eight-noded quadrilateral elements. For elements with a discontinuity, the integration scheme needs to be adjusted in order to integrate the tractions at the discontinuity. Figure 3 shows a four-noded quadrilateral element with the discontinuity along side \overline{jk} and the augmented integration scheme. It is stressed that, even if the discontinuity is placed along the common boundary of two elements (see Figure 2), the traction law is integrated only along the side \overline{jk} of the interface-like element. A the Gauss integration scheme has been used for the integration over the continuum Ω^e and on the discontinuity Γ_d^e .

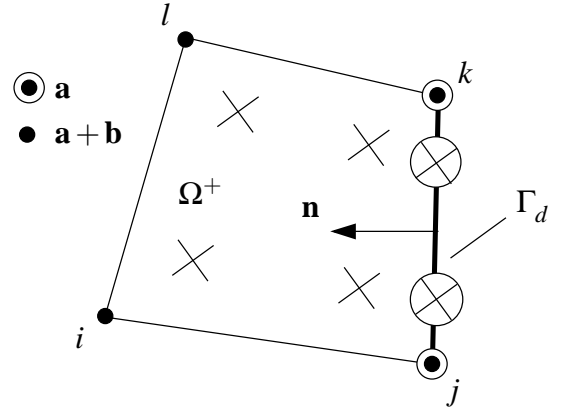


Figure 3: Integration scheme and degrees of freedom for an interface-like four-noded quadrilateral element.

Since the gradient-enhanced damage model requires an extra interpolation field for the non-local equivalent strain (Peerlings 1999), the Heaviside jump is chosen to be non-zero on displacement-based continuum elements. For this reason, in the analysis of a reinforced brittle material, in which the concrete is described by a gradient-enhanced damage model, the displacement jump was added to the nodes of the element representing the reinforcement.

Although it is possible to activate a discontinuity after a specific condition is met (Wells and Sluys 2001b), here it is assumed that the discontinuity is considered to be present from the beginning of an analysis. This keeps the implementation relatively simple and allows for a direct comparison with standard interface elements.

6 APPLICATIONS

The performance of the method is examined by means of two examples. The first application illustrates the ability of the interface-like element in reproducing the rigid solution. This is a critical issue in numerically integrated continuous interface elements. The second application examines the pull-out of a steel fibre from a concrete matrix.

6.1 Two-dimensional linear elastic analysis of a notched beam

The performance of the numerical procedure is investigated for the two-dimensional notched beam depicted in Figure 4. This test was used by Rots (1988) to test the performance of numerically integrated continuous interface elements. Four noded quadrilateral elements are used under plane stress conditions. A Young's modulus of 20000 N/mm^2 and a Poisson's ratio of 0.2 have been used for the continuum part. Interface-like elements, shaded in Figure 4, have been added in front of the notch. To reproduce a pure mode-I opening, only displacement jumps in the horizontal direction are activated. The analyses reported

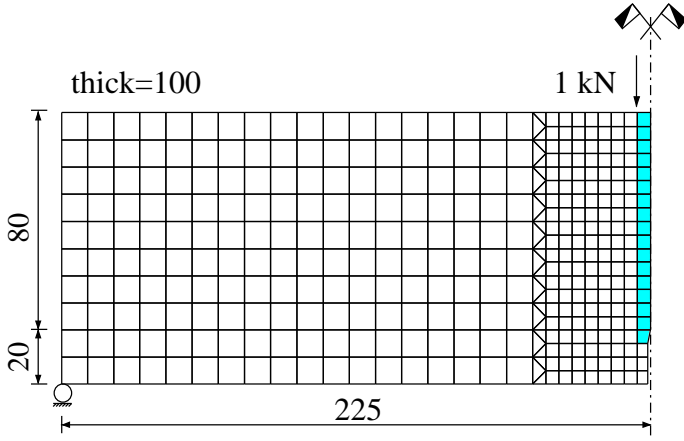


Figure 4: Mesh for linear interface analysis of a notched beam (dimensions in mm).

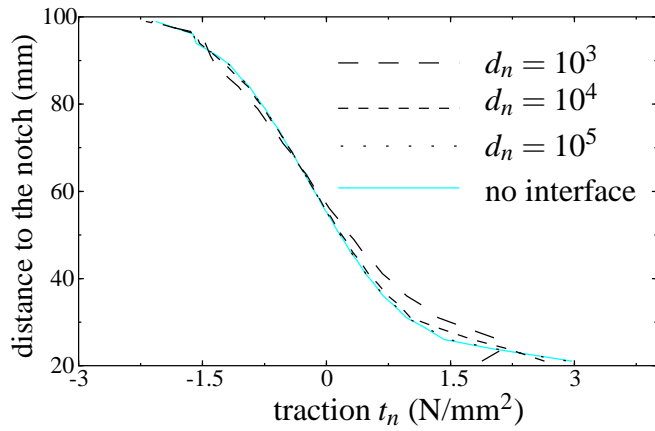


Figure 5: Traction profile in front of the notch of the beam.

by Rots show a normal traction profile along the central line of the beam which is highly dependent on the stiffness of the interface and on the chosen numerical integration scheme. In particular, it was shown that high values of the normal stiffness lead to significant oscillation of the normal traction profile.

The ability of the partition of unity method to reproduce the correct traction profile is shown in Figure 5, in which the tractions have been sampled at the integration points at the discontinuity. The stiffness d_n at the discontinuity ranges from 10^{+3} to 10^{+5} N/mm^3 . To achieve a negligible separation in the initial uncracked state and to capture the high traction gradient ahead of the notch it is suggested that a good estimate of the initial discontinuity stiffness d_n could be of the same order as the stiffness of the surrounding continuum. As shown in Figure 5, for $d_n = 10^{+5}$ N/mm^3 the traction profile of the rigid solution is reproduced exactly. It is stressed that higher values of d_n result in a traction profile that is *indistinguishable* from the rigid one, and no stress oscillations are observed.

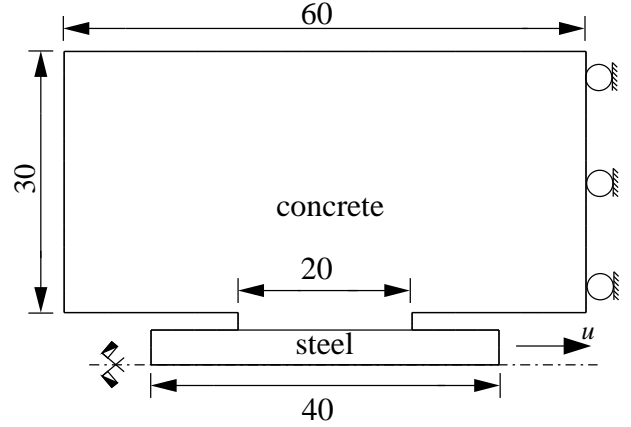


Figure 6: Geometry of the pull-out specimen (dimensions in mm).

6.2 Pull-out modelling

The non-linear behaviour of the interface-like element has been examined by analysing a pull-out test of a steel fibre with a short embedment length (see Figure 6). The fibre is loaded by a prescribed displacement incrementally applied at the right end. The simulations have been performed under plane strain condition using eight noded quadrilateral ele-

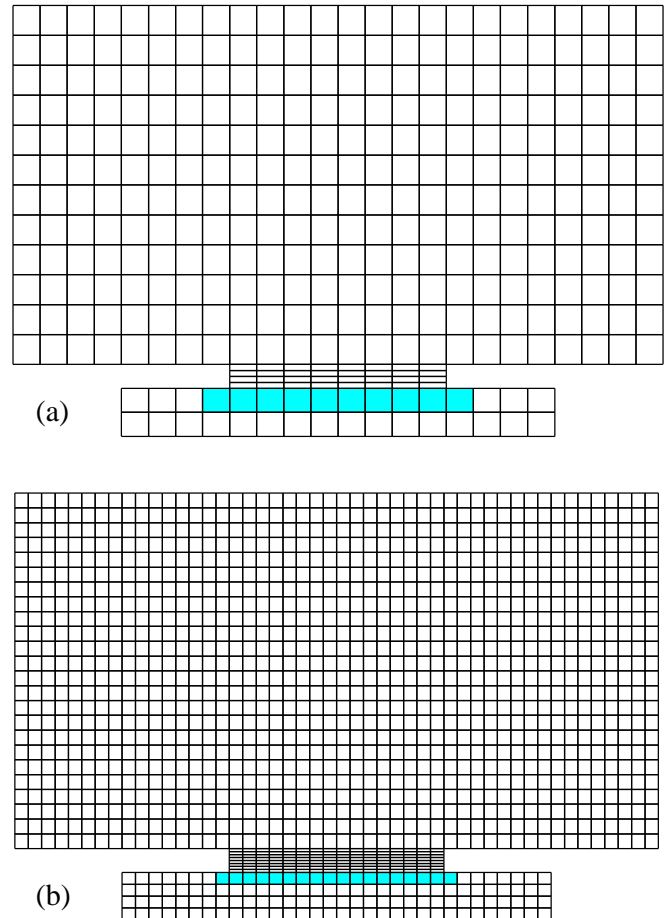


Figure 7: Meshes for the pull-out test: (a) 352 elements; (b) 1408 elements. Interface-like elements are shaded grey.

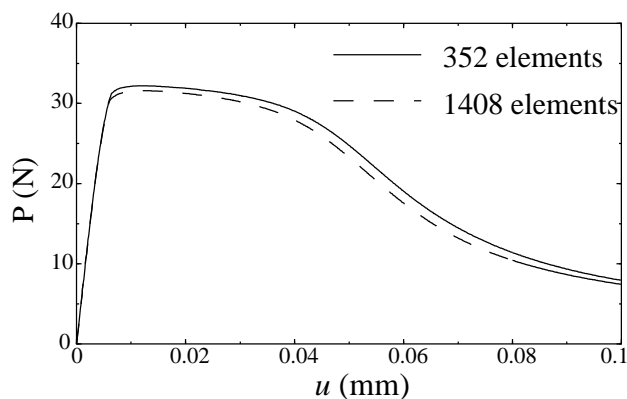


Figure 8: Load displacement curve for the pull-out test.

ments. The cementitious matrix is modelled using a gradient-enhanced damage model. Young's modulus of 20000 N/mm^2 and a Poisson's ratio of 0.2 have been used for the cementitious matrix. The gradient parameter has been set to 1 mm^2 and a value of 10 for the ratio of the compressive and the tensile uniaxial strength in the Modified von Mises equivalent strain definition has been used (see Peerlings (1999) for details on the gradient-enhanced continuum model). For the steel fibre, linear elastic behaviour with Young's modulus of 200000 N/mm^2 and a Poisson's ratio equal to zero are used. The damaging interface model in equation (20) with $d_s = 200000 \text{ N/mm}^3$, $\kappa_i = 8 \times 10^{-6} \text{ mm}$ and $\kappa_u = 100 \text{ mm}$ has been used for the shaded elements in Figure 7. The load-displacement curve depicted in Figure 8 shows the objectivity of the model with respect to spatial discretisation and a near-horizontal plateau in the load-displacement response just post the peak load. This is typical of pull-out tests.

7 CONCLUSIONS

The use of the partition of unity method to develop an interface-like element has been considered. The displacement field is enriched with the Heaviside jump function, thus providing the natural environment to describe fibre pull-out failure in concrete. It is emphasized that the method is suitable for any class of problems in which a material discontinuity is expected.

A limitation of numerically integrated continuous elements is the difficulty in reproducing the rigid solution. Moreover, the presence of stress oscillations introduces undesirable difficulties in non-linear computations. It has been shown that this method can successfully overcome these deficiencies. The two-dimensional linear elastic analysis of a notched beam showed that this method is able to reproduce the rigid solution.

Further, it is important to note that no additional elements are required to model a discontinuity; only extra degrees of freedom are added to the nodes that correspond to the interface. The ability of the method

to properly model interface behaviour makes it a valuable tool for the analysis of reinforced brittle materials.

ACKNOWLEDGEMENTS

Financial support through the programme BEO (special fund from TU Delft for excellent research) is gratefully acknowledged. Financial support for the second author from the Netherlands Technology Foundation (STW) is gratefully acknowledged.

REFERENCES

- Melenk, J. M. and I. Babuška (1996). The partition of unity finite element method: Basic theory and applications. *Computer Methods in Applied Mechanics and Engineering* 139(1–4), 289–314.
- Peerlings, R. H. J. (1999). *Enhanced damage modelling for fracture and fatigue*. Ph. D. thesis, Eindhoven University of Technology.
- Rots, J. G. (1988). *Computational modeling of concrete fracture*. Ph. D. thesis, Delft University of Technology.
- Wells, G. N. and L. J. Sluys (2001a). Discontinuous analysis of softening solids under impact loading. *International Journal for Numerical and Analytical Methods in Geomechanics* 25(6).
- Wells, G. N. and L. J. Sluys (2001b). A new method for modelling cohesive cracks using finite elements. *International Journal for Numerical Methods in Engineering* 50(12), 2667–2682.